Symmetry and Geometry of the Face on Mars Revealed

A New Analysis Based on the April 2001 Image

Mark J. Carlotto, Ph. D.

Abstract

On April 8, 2001 Mars Global Surveyor (MGS) was able for the first time to obtain a fully illuminated high resolution image of the Face on Mars. Like previous MGS images the Face appears at first glance to be a highly eroded natural formation. However analysis of this new image shows the object to possess a very high degree of symmetry in two directions. Using repeatable geometrical constructions based on clearly resolved features the Face appears to fit a consistently expressed geometrical model based on rectangles having a long to short side ratio of 4/3, i.e., by rectangles diagonally bisected by 3-4-5 right triangles. Analysis of the new image reveals that the right (east) side of the Face is covered with sand. The depth of the sand appears to be sufficient to have covered over some of the detail on the east side and may account for its apparent lack of facial symmetry.

1. Introduction

The Face on Mars is a mile long formation on the surface of Mars that resembles a humanoid face. First photographed by a Viking Orbiter spacecraft in July 1976, the Face was dismissed by NASA's Jet Propulsion Laboratory as an optical illusion -- a rock formation that happened to look like a face because of the way it was lit by the sun (JPL 1976). Several years later two engineers at the Goddard Space Flight Center (DiPietro and Molenaar 1986) found a second image of it taken at a different sun angle that also exhibited facial characteristics. Using these images a 3-D model was constructed and used to show the Face is not an optical illusion as claimed by NASA but appears face-like over a wide range of lighting conditions and imaging geometries (Carlotto 1988). It was also shown to contain fine scale facial detail and to be highly non-fractal and possibly non-natural in structure (Carlotto and Stein 1990).

A high resolution image taken by the Mars Global Surveyor (MGS) in April 1998 revealed the Face to be highly eroded. Although JPL maintains the Face is a natural formation, no different from other landforms in Cydonia (Pieri 1999), close examination of the MGS image not only corroborated the presence of many of the details first seen in the Viking data but also confirmed the overall structure of the Face to be highly symmetrical (Carlotto and Brandenburg 1998).

Historically, most of the debate over the Face has revolved around subjective judgments of its face-like characteristics. Critics state the Face cannot be a face and thus cannot be artificial because it doesn't look like a face. Clearly if a more quantitative measure of artificiality existed an objective assessment could be made. Because artificial objects tend to be symmetrical, symmetry is a powerful criterion for assessing the artificiality of objects. The problem has been that because the Face had not been imaged in its entirety, assessments of its symmetry were incomplete and conjectural.

In April 2001, the Mars Global Surveyor (MGS) was able for the first time to obtain a fully illuminated high resolution image of the Face. This paper provide the first complete analysis of the symmetry and geometry of this enigmatic feature -- one that strongly suggests that it is an artificial object.

2. On The Symmetry of the Face

In 1983 an independent review of the Viking data was performed by a group of scientists and engineers outside of NASA (Pozos 1986). As part of this investigation the Face was found to be a well proportioned and highly symmetrical object (Hoagland 1996). Analysis of the April 1998 MGS image confirmed this (Brandenburg and Carlotto, 1998). Using registered and orthorectified images (see Appendix B for a discussion of othorectification) from Viking frame 70A13 and the April 1998 MGS image, the positions of the left and right bases, left and right edges of the platform, and centerline of the Face were measured (Figure 1). The centerline was established by running a line from between an 'X' pattern on the top of the head, down along the ridgeline defined by the points of highest elevation on the formation, between two circular features resembling nostrils, and down through the middle of the mouth. The measurements were then averaged to obtain estimates for the horizontal (lateral) position of the left and right bases, left and right edges of the platform, and the centerline. The distances between the centerline and the left and right platform edges were found to differ by about 8%. Using the distances between the centerline and left and right bases, which are better defined, the Face was found to be even more symmetrical with the two sides differing by only 1% -- well within measurement error.
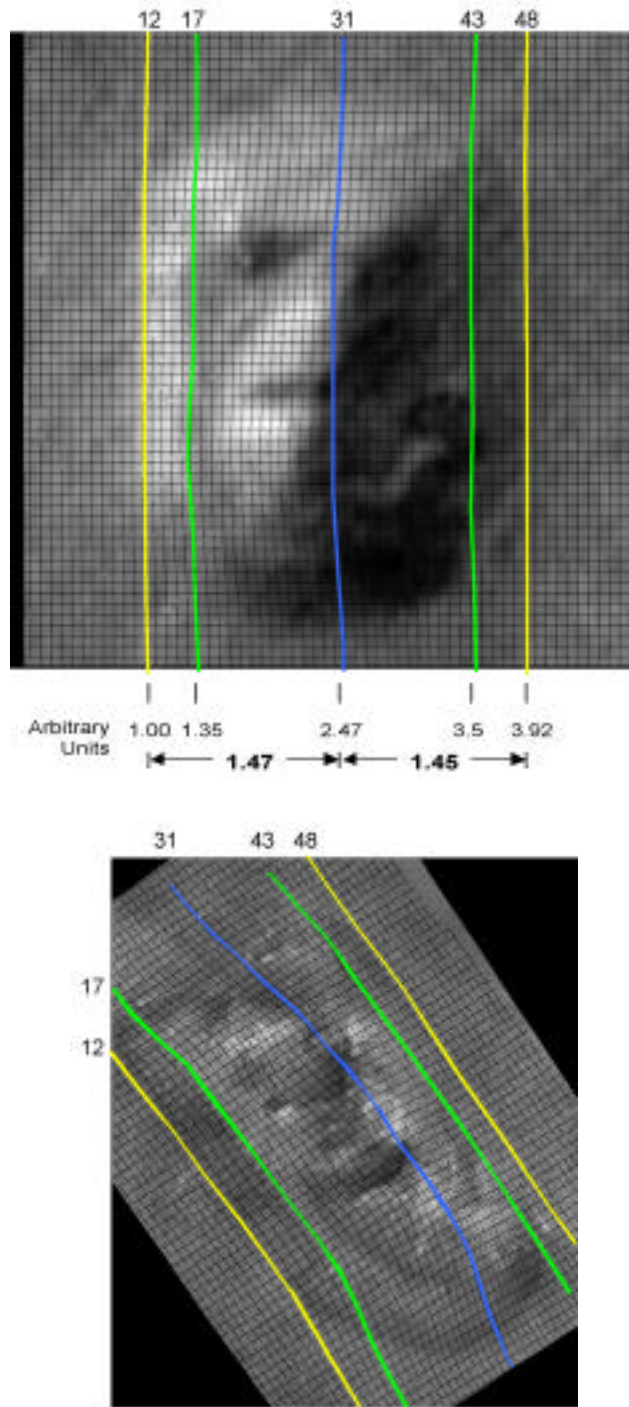
Figure 1 Edges of base and platform, and centerline delineated in orthorectified 70A13 coordinate system (above) and corresponding MGS coordinate system (below).

In Viking frames 35A72 and 70A13 the sun was to the northwest and low enough in the sky to shadow most of the right (east) side of the Face. Because MGS was aimed 45 degrees off angle to image the Face very little of the right side of the Face was visible. But even though the right side of the Face had not been observed in its entirety, it did not seem to match the left. This lack

of symmetry has caused many to dismiss the Face as a natural geological landform. But in assessing possible ancient artifacts (terrestrial or otherwise) it seems both reasonable and necessary to assume that a certain amount of degradation would have occurred over time. Erjavec and Brandenburg (1999) have found what appear to be rills -- runoff channels -- on several Cydonian landforms. This is strong evidence that these features were aerially exposed and that erosion occurred through the actions of both precipitation and surface runoff.

In an attempt to explain the fact that the two sides of the Face are different, it has proposed that the two sides of the Face are different facial representations (Sirisena 2001). By taking each side and its mirror image it is possible to create two faces -- one being that of a hominid, the other having feline characteristics. Although this is one possible explanation there is no compelling terrestrial precedent for such a representation.

Although manmade features on the surface of the Earth come in a variety of shapes and sizes, most are symmetrical in shape. Because artificial objects tend to be symmetrical, symmetry is a powerful feature for detecting artificial objects in remotely-sensed imagery. Zabrodsky, et. al. (1995) define the concept of symmetry distance to be the minimum 'effort' required to transform any given shape into a symmetrical shape. For a set of points, the effort is related to the amount each point must be moved from its location in the original shape to that in the symmetrical shape. It seems reasonable to assume that the amount of effort, in an erosional sense, required to transform a given landform into a symmetrical landform can be used as a means of assessing the possible artificiality of the landform.

Using this idea, let us consider the possibility that, at one time, the Face might have possessed a much higher degree of internal symmetry than it does today, and that erosion might be responsible for its present condition (Figure 2). Three obvious asymmetries are evident in the imagery:

> Right eye - Is it possible that the right eye structure might be covered by debris that has slid, slumped, or toppled down from what would have been the right extension of the brow ridge? The edge of a debris flow could account for the bright region below where we would expect the eye to be in the MGS image, and the light region seen in the Viking image just below the dark area that gives the impression of the right eye.

> Light colored crescent-shaped structure below and to the right of the chin - The shape suggests a dune, perhaps from windblown material deposited on the leeward side of the Face. Light colored material on the lee of an object could be indicative of dust deposited by the wind. Above 40° N the prevailing wind direction is from the west (Carr 1981). As the left side of the Face appears darker it is possible that light colored material is being

eroded from the left and deposited on the right side of the Face. Mass wasting is another possible explanation for this feature whereby the material has either slid or slumped down from the right side of the central ridge.

Right side of mouth - The lack of strong shadows on the right side of the Face suggests that the mouth does not extend across the face. But on closer examination subtle outlines do seem to be present. Could the right side of the mouth depression be filled in by the same windblown material forming the dune just below it?

The hypothesis that the Face might have once been much more symmetrical than it is at present seemed both plausible and testable based on analysis of the April 1998 MGS image. All that was required was another image showing the right side in full illumination.

3. Data Processing and Analysis

In response to continued interest in the Face, MGS was finally able to obtain a fully illuminated high resolution image of it on April 8, 2001. At 8:54 PM (Greenwich time zone) as MGS descended from Mars' north pole the spacecraft was rolled 24.8° to the right to image the Face 165 km to the west at a distance of about 450 km. A 2048 x 6528 pixel image strip (designated E03-00824) was collected with a ground resolution of about 2 meters per pixel.

After downloading the raw data from the Malin Space Science System (MSSS) web site, the first step in our analysis was to crop the raw image to a 2048 x 2048 pixel region containing the Face. The Mars Orbiter Camera (MOC) creates an image by sweeping a 1-D detector array (line scanner) over the surface in time. Vertical striping in the raw image caused by gain variations between elements in the MOC detector array was removed by dividing each column in the image by the average brightness of the column and multiplying by a constant to map the resultant dynamic range to 0-255.

Because of the off-angle imaging geometry the image was orthorectified to correct for geometrical distortions in the raw MGS image (Appendix B). First a digital elevation model (DEM) was computed using a single image shape-from-shading (SFS) algorithm (Appendix A). SFS provides a high resolution DEM that is precisely registered to the image. The DEM was then used to re-project the image to appear as if it were acquired from directly overhead. The raw and destriped orthorectified images are shown in Figure 3.
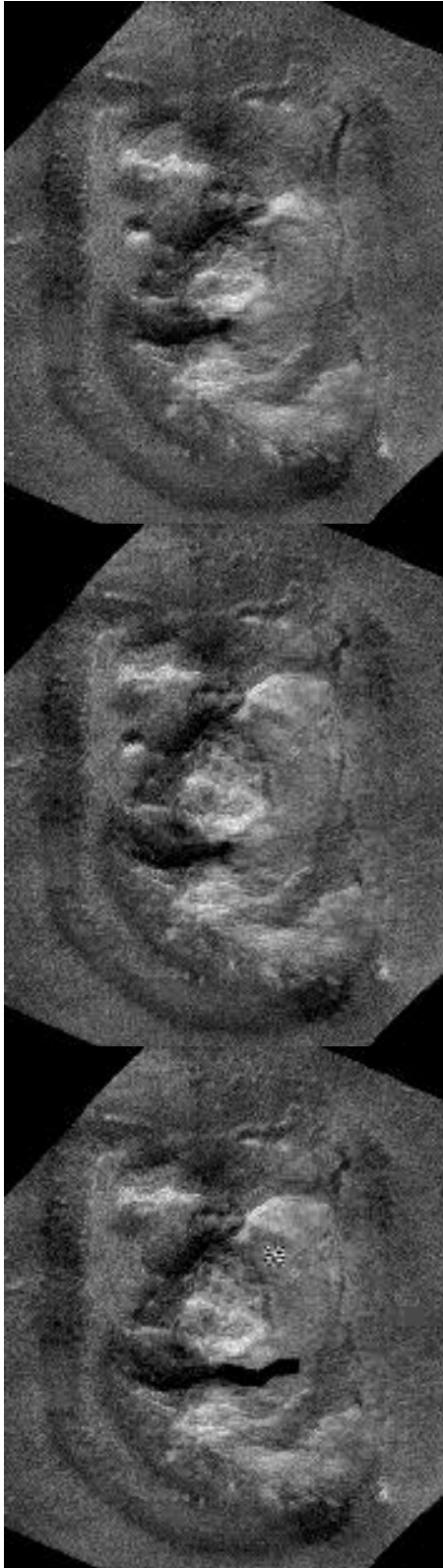
Figure 2 Notional reversal of the erosional process. Orthorectified MGS image (left). Speculative reconstructions follow: Reversing possible mass wasting event raises right eye (below left). Removing material possibly deposited in mouth reveals right extension (below right). Rubble on left side which may have slid down from nose ridge of face removed (bottom left). Dune formed from windblown material deposited on lee side of face below right side of chin removed (bottom right).
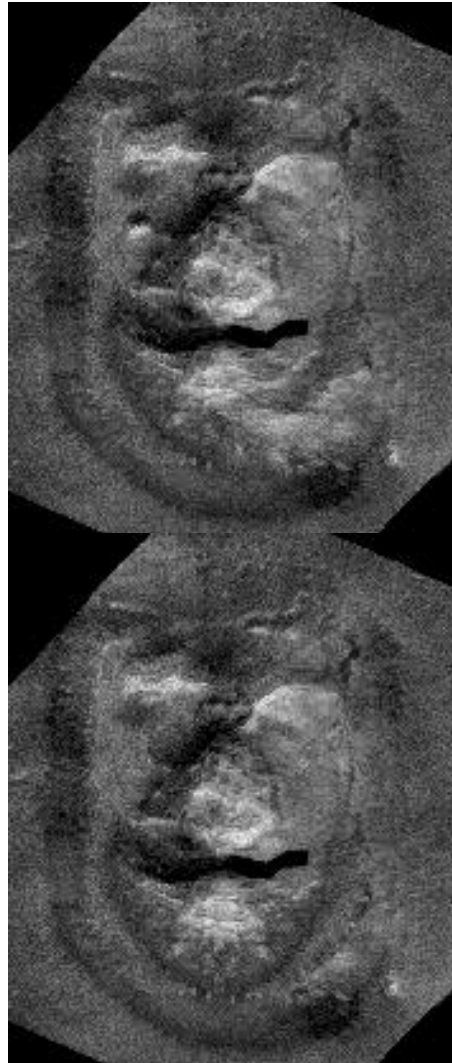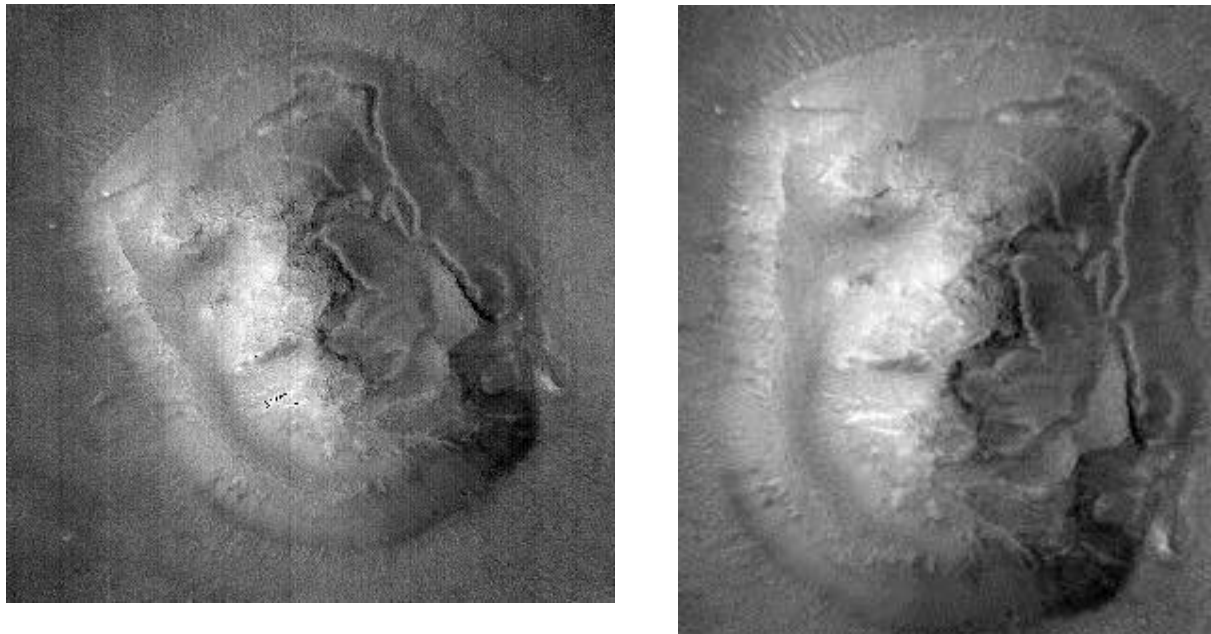
Figure 3 Portion of raw MGS image E03-00824 (left) and destriped orthorectified image (right)

We employed a symmetry measure proposed by Marola (Appendix C) to locate horizontal and vertical axes of symmetry. His measure is based on the normalized difference between an image and its reflection about a given axis of symmetry. Figure 4 plots the horizontal and vertical symmetries of the Face for different hypothetical axes of symmetry. Peak locations give the axes of symmetry. Note that the axes of symmetry of the DEM are displaced down and to the right relative to those of the orthorectified image. The reason for this may be due to an accumulation of sand on the leeward side of the Face which would effectively shift the center of mass (and axes of symmetries) south and east.
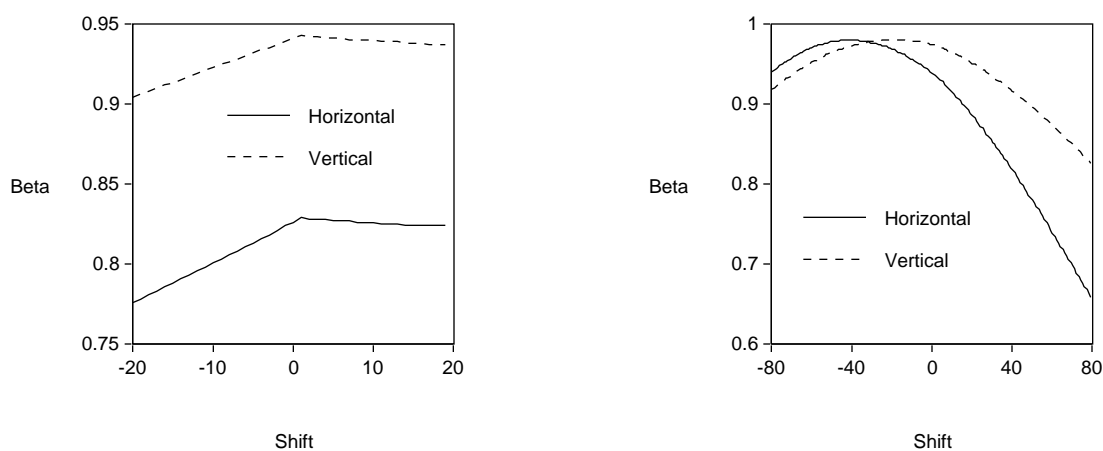

Figure 4 Marola symmetry measure plotted for different horizontal and vertical shifts of the orthorectified image (left) and DEM (right).

Figure 5 presents the orthorectified image shifted so that its center coincides with the intersection of its horizontal and vertical axes of symmetry. This point is in the center of a circular feature **a** which appears to be a slight depression in the surface. The lateral axis of symmetry (vertical line) passes through this and three other more or less regular circular features **b-d** (Figures 6 and 7).
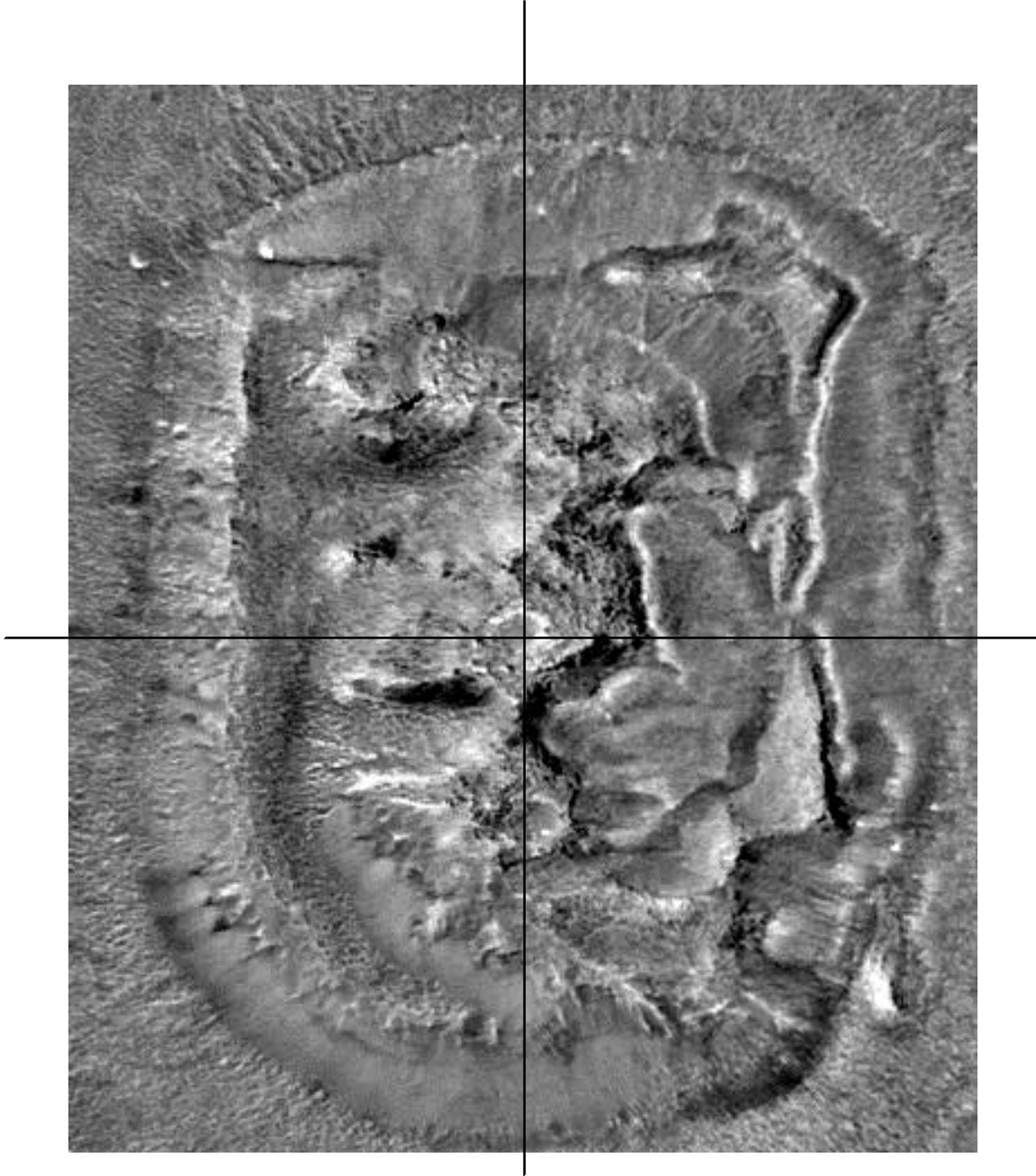

Figure 5 Orthorectified image with vertical and horizontal axes of symmetry shown. Note the two axes intersect at the center of a small circular depression.
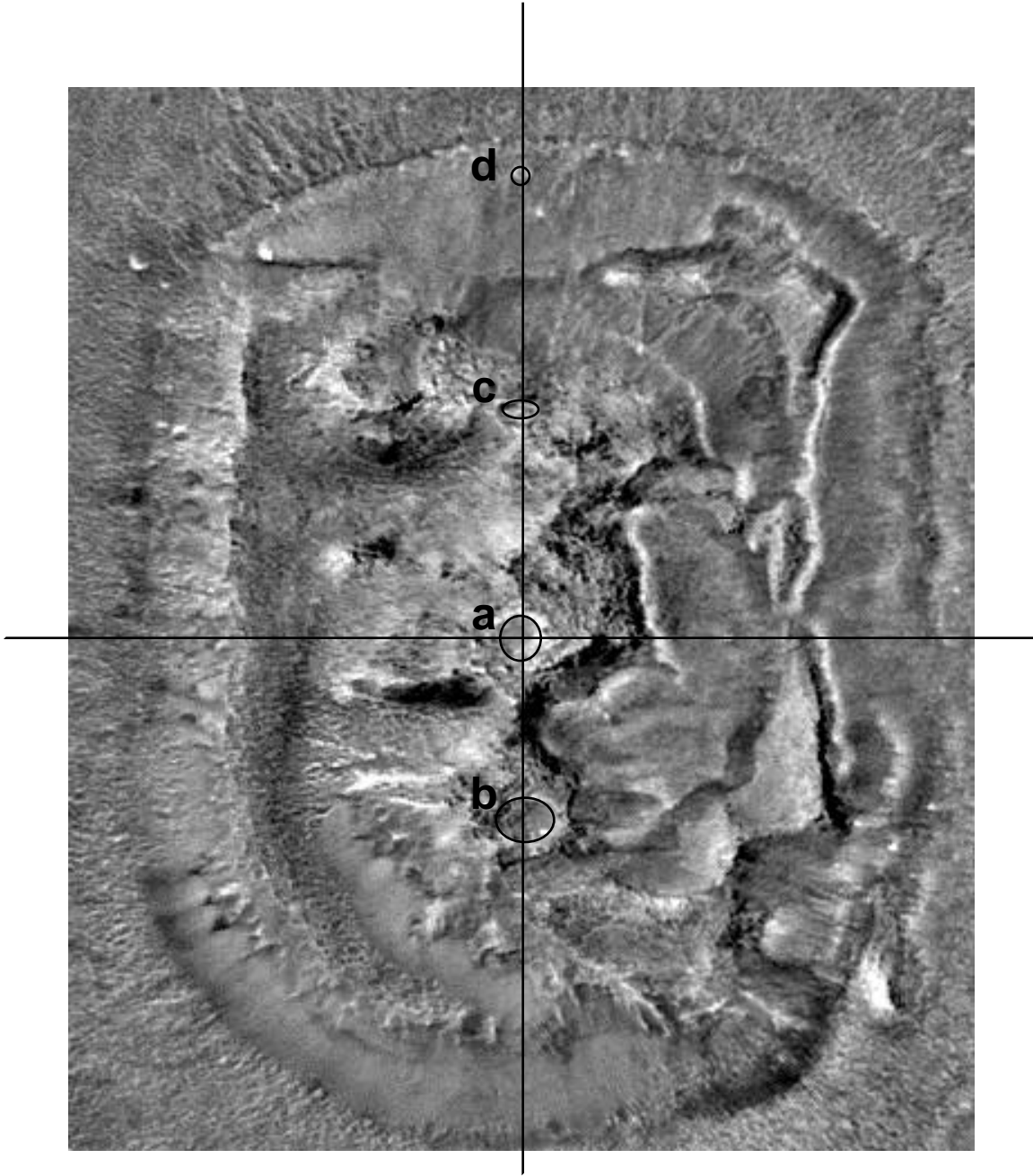
Figure 6 Four circular features (a-d) located along the lateral centerline (horizontal axis of symmetry).
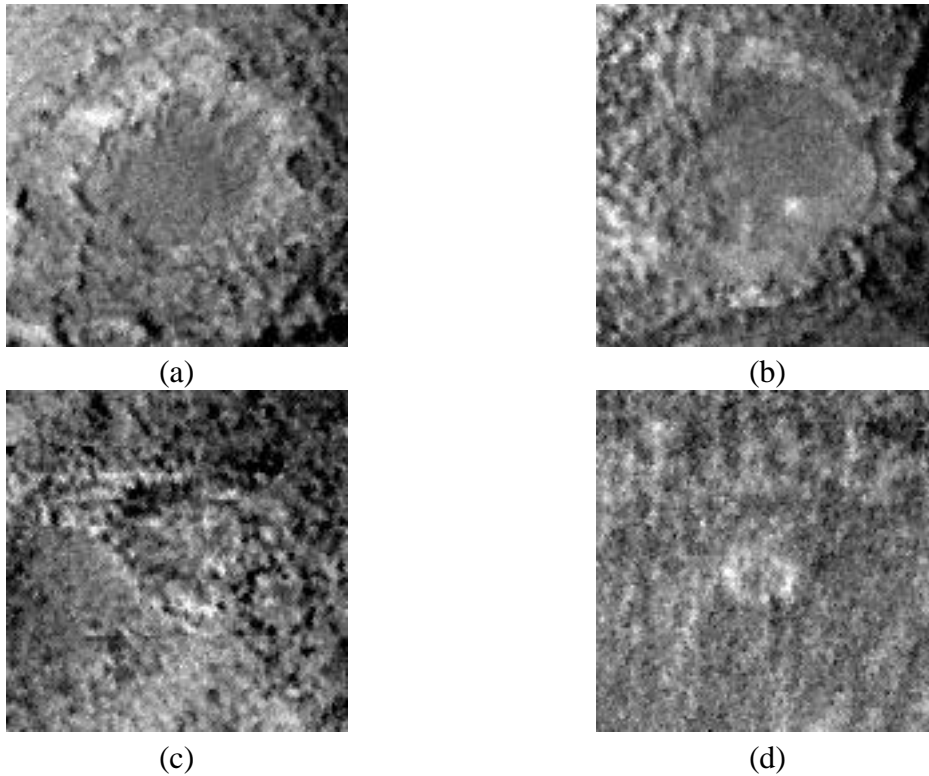
(a)

(b)

(c)

(d)

Figure 7 Close up of circular features along lateral centerline of the Face

The Face consists of a raised platform defined by a beveled edge. Examination of the shape of the bottom left edge of the base of the platform shows it to conform to a conic section, specifically to a segment from an ellipse of eccentricity e~0.22 (Figure 8). The top of this ellipse **e1** passes through one of the circular features **c** identified in Figure 6. A rectangle can be constructed whose left and bottom sides are tangent to the ellipse and opposite vertex is in the center of the central depression **a**. Three other rectangles of exactly the same size can be constructed using **a** as the common vertex. All four rectangles have an aspect ratio of 4 to 3; i.e., they are bisected by triangles whose sides are 3, 4, and 5 units long. The union of the four rectangles is also a 4-3 rectangle and is denoted **E-F-G-H** in Figure 10. Within this rectangle we can inscribe an ellipse **e2**. The four points where this ellipse intersects the two diagonals of the **E-F-G-H** rectangle define the four vertices of another rectangle denoted **A-B-C-D**. This is also a 4-3 rectangle and is exactly one half the area of **E-F-G-H**. As seen in Figure 8 these two rectangles neatly define the beveled edge on the left side of the Face and bound its extent at the top and bottom.
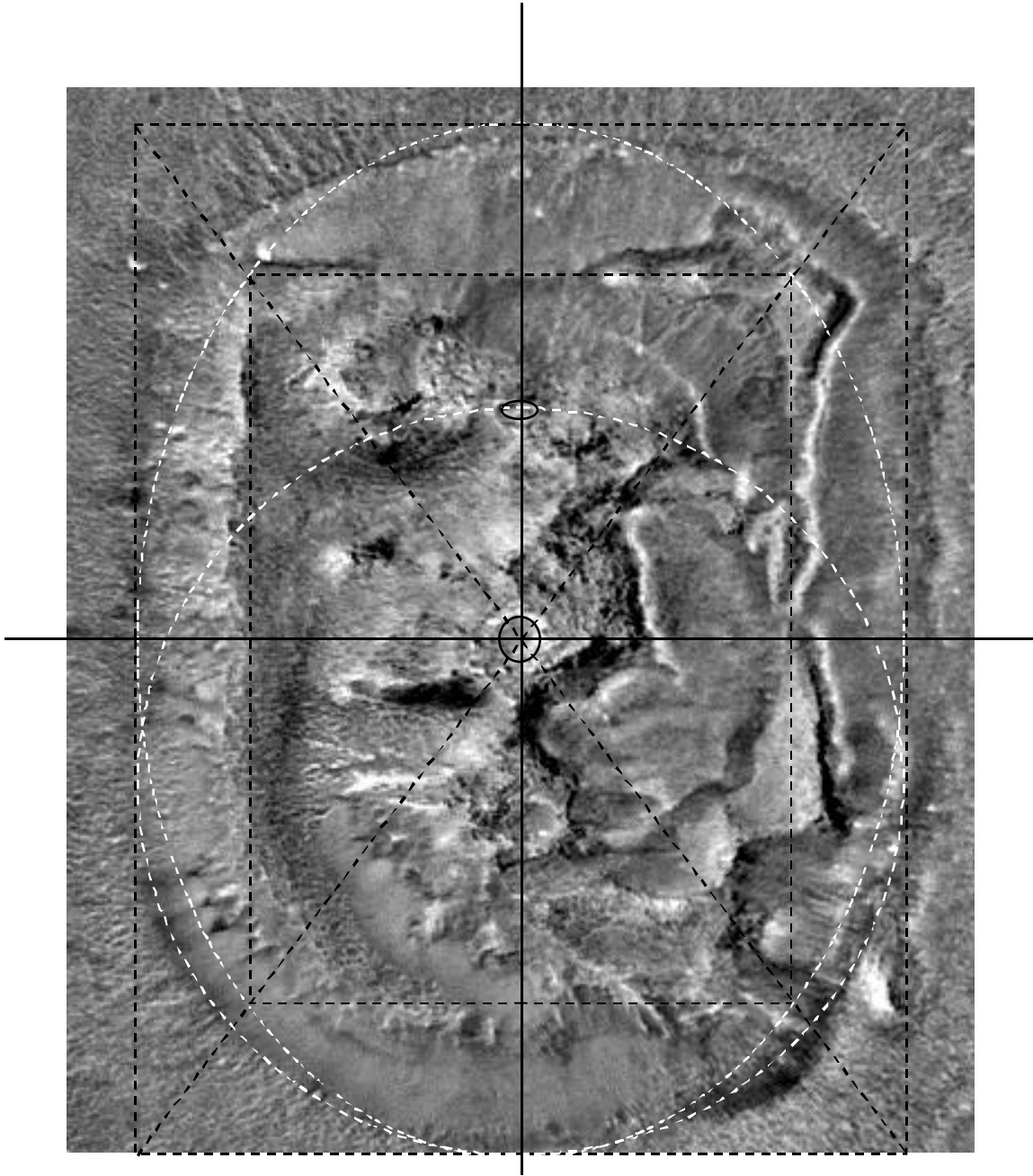
Figure 8 Geometrical construction of inner and outer 4-3 rectangles (see Figure 10 for a key to the overlays).

We performed an independent construction to assess the consistency of this simple yet elegant 4-3 geometry. With reference to Figure 9, we can fit an ellipse **e3** to the top left edge of the base of the platform. This ellipse passes through the center of another one of the circular features **b** located along the lateral axis of symmetry. The area of this ellipse is very close (within 0.3%) to the area of ellipse **e1** which frames the bottom of the base in Figure 9. Within this ellipse one can inscribe an ellipse between the two previous ellipses that passes through circular features **b** and **c**

and is tangent to **A-B-C-D**. This ellipse has an aspect ratio of 4/3 (i.e., is bounded by a 4-3 rectangle) and is offset from the vertical axis of symmetry. The ratio of the distance from the axis to the top of **e4** to the distance from the axis to the bottom of **e4** is about 4/3 (to within 3%).
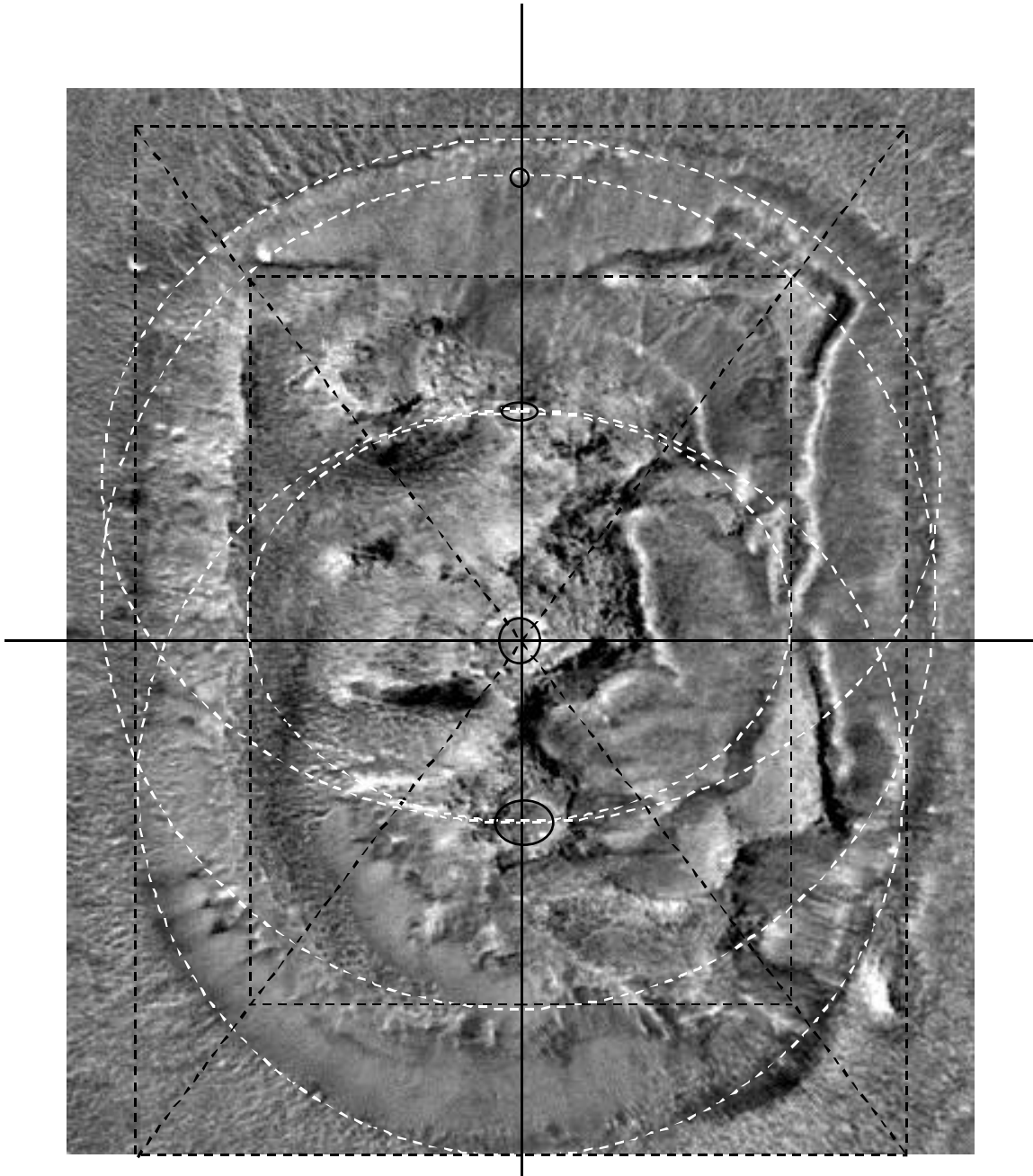

Figure 9 Additional support for 4-3 rectangles (see Figure 10 for a key to the overlays).

We note several other planimetric relationships. First, along the upper left diagonal, ellipse **e1** intersects the line halfway between the point where ellipse **e3** intersects the line and the center. This occurs near a feature which, under certain lighting conditions, casts a shadow that gives the

impression of an eye. Second, the distances **a-c** and **d-c** are equal (within measurement error). Third, a circle can be drawn that touches the bottom of **A-B-C-D** and its two top vertices **A** and **B**. This circle passes through the fourth circular feature **d**. Another circle with the same size can be drawn that touches the top of **A-B-C-D** and its two bottom vertices **C** and **D**; however there is no feature visible corresponding to **d** at the bottom.
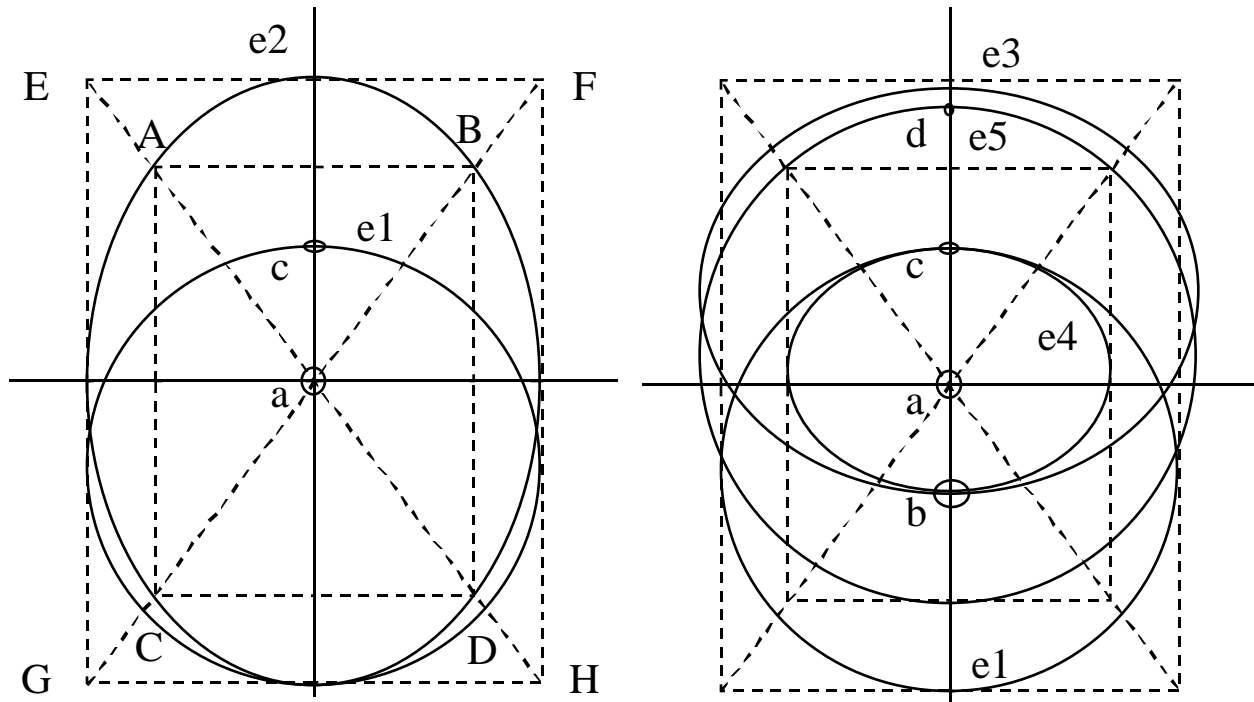
a) Circular features (a,c) along horizontal axis of symmetry. Outer rectangle E-F-G-H consisting of 4 smaller rectangles with vertices at E, F, G, and H, and sharing a common vertex a. Ellipse e1 fit to bottom edge of platform used to construct outer rectangle. Ellipse e2 inscribed in outer rectangle. Inner rectangle A-B-C-D inscribed in ellipse e2.

b) Circular features (a-d) along horizontal axis of symmetry. Ellipse e1 fit to bottom edge of platform used to construct outer rectangle passes through circular feature c. Ellipse e3 fit to top edge of platform passes through circular feature b. Areas of e1 and e3 are about the same. Ellipse e4 passes through b and c and is tangent to inner rectangle. Circle e5 passes through circular feature d, inner rectangle vertices A and B and is tangent to bottom of A-B-C-D.

Figure 10 Keys to overlays in Figures 8 and 9.

Careful examination of the image provides additional evidence supporting the hypothesis that the Face is a highly symmetrical and geometrically regular structure. The top corners of the **A-B-C-D** rectangle frames two rounded corners on the Face. As shown in Figure 11 the corners also appear to have the same 3-D shape.
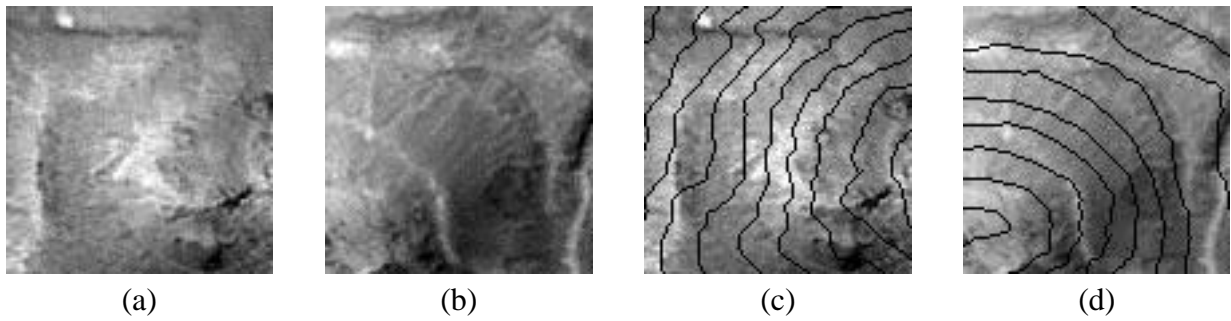
Figure 11 Upper left (a) and right (b) corners of top of platform. Elevation contours (c) and (d) suggest a similarity and symmetry in the underlying surface as well.

As shown in our constructions, the right edge of the **E-F-G-H** rectangle lies to the left of what appears in the image to be the base of the beveled edge. Comparison of profiles taken from opposite sides suggest that the base does in fact coincide with the right edge of the **E-F-G-H** rectangle (Figure 12). The impression that the base is to the right is created by a build up of sand at the base. A 3-D perspective view from below the chin created by mapping the orthorectified image onto its DEM (Figure 13) indicates the presence of sand dunes on the east side of the Face. The depth of the sand appears to be sufficient to have covered over some of the detail on the east side. The presence of the sand also accounts for the difference between the lateral axes of symmetry of the image and its DEM.
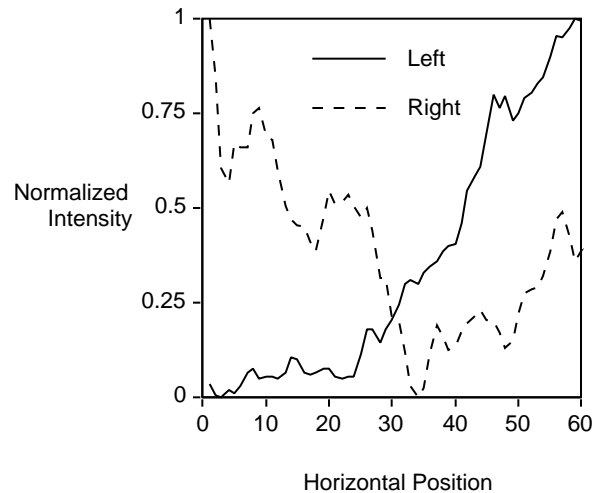

Figure 12 Shifted and superimposed horizontal intensity profiles across the left and right base of the platform. Negative correlation (r=0.79) from 0-35 indicates presence of correlated edge structure on opposite sides of the platform. Positive correlation (r=0.76) from 35 to 60 is consistent with a build up of sand at the base on the right side.
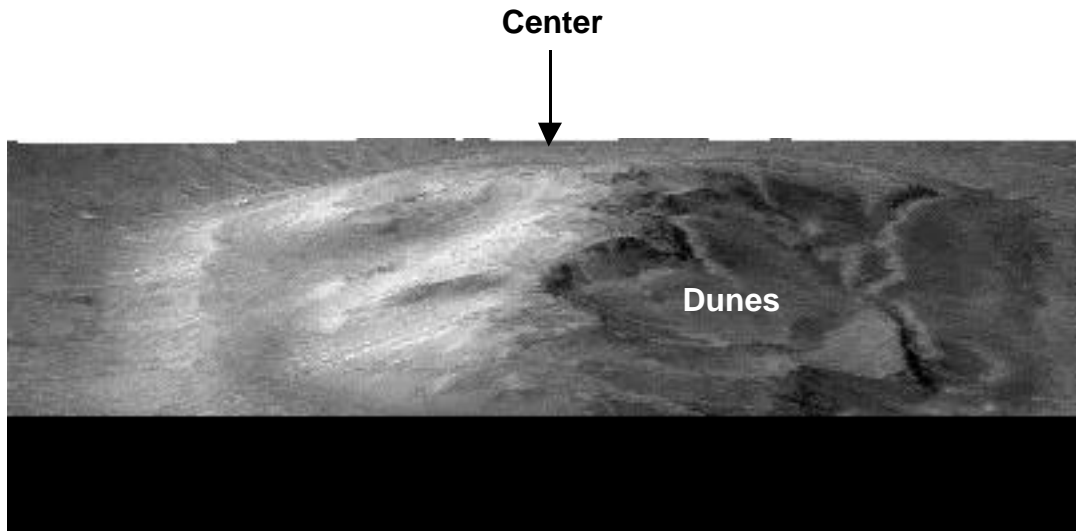
Figure 13 Perspective view from below the chin showing dunes on east side

4. Discussion

The location and spacing of features **a**-**c** establish the 4-3 rectangular geometry of our model of the Face (Figure 14):

- The intersection of the horizontal and vertical axes of symmetry and the centers of rectangles **A-B-C-D** and **E-F-G-H** -- both 4-3 rectangles -- lie within **a**.

- The intersections of ellipses **e1** and **e3** which bound the edges at the base of the platform and the horizontal axis of symmetry fall inside **c** and **b**. The ratio of the center-to-center distances **a**-**b**/**a**-**c** is approximately 4/3 (to within 3%).

- These same two points of intersection within **b** and **c** together with rectangle **A-B-C-D** define another 4-3 rectangle which bounds ellipse **e4**

In order to assess the statistical significance of our model we compute the likelihood that a particular configuration of features is random (Appendix D). It is shown that the likelihood depends on how precise we require the configuration to be, how many features are involved in the configuration, and how many total features are present from which to choose. The odds that three points lie within circular areas of the size of **a**, **b**, and **c** is shown in Appendix D to be on the order of one in a million. That they lie near the centers of these regions is extraordinary.
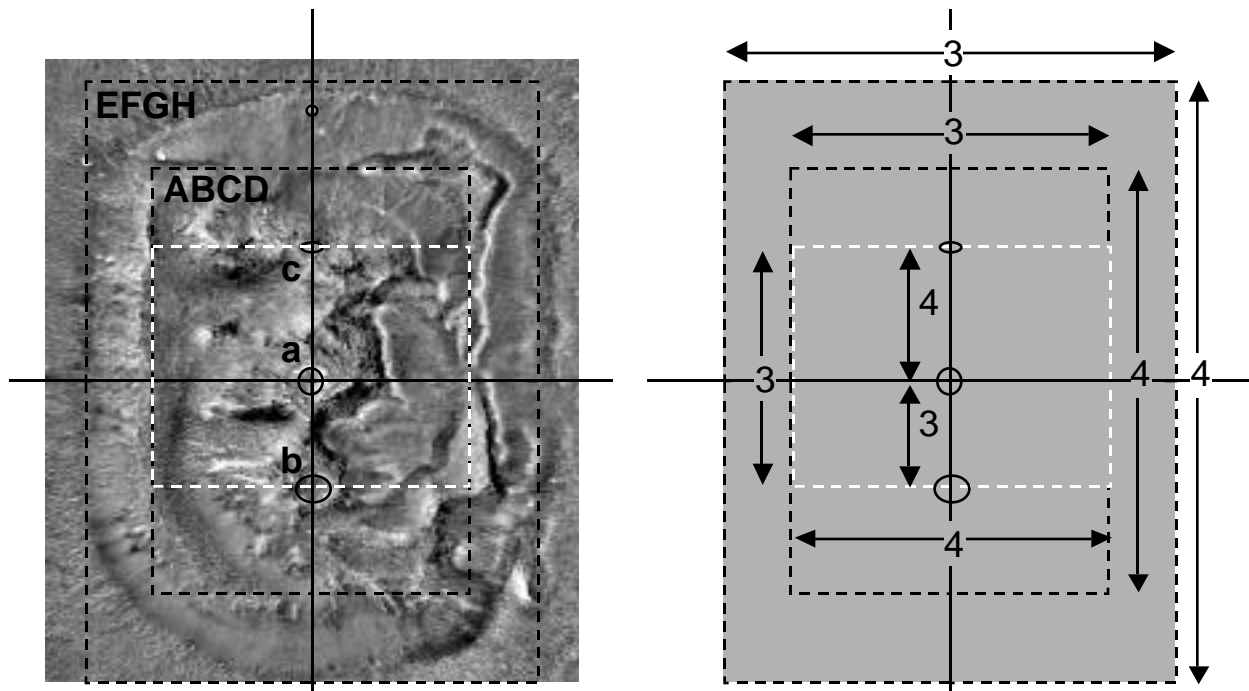
Figure 14 Shape of Face appears to conform to underlying geometry based on 4-3 rectangles

Although it can be argued that the likelihood that any particular spatial configuration occurs at random decreases as the number of features in the configuration (number of degrees of freedom) increases, the geometric complexity of the configurations will also tend to increase; i.e., they will not in general conform to a consistent, redundantly expressed geometry. That the locations of the circular features lie as they do in relation to the rest of the Face so as to repeatedly suggest an underlying geometry based on 4-3 rectangles is difficult to explain by chance.

Early in the 19th century the great German mathematician, Karl Gauss proposed that the universal language of mathematics, in particular the Pythagorean theorem be used as the basis for extraterrestrial communication (Ley 1951). His idea was to plant tracts of pine forest in Siberia to enclose a huge right triangle with wheat growing inside. In summer the light colored wheat would strike a contrast to the dark green of the trees while in winter snow inside would stand out from the trees. The idea was to create a 'signal' large enough on the earth's surface to be seen from space. The triangles formed by diagonally bisecting 4-3 rectangles are 3-4-5 right triangles. It is interesting to note that knowledge of the 3-4-5 triangle predates the Pythagorean theorem by thousands of years and was well known to the Caldeans, Babylonians, and Egyptians.

Although the significance of this last statement is open to debate, most would agree that artificial objects tend to be symmetrical and are often rectangular in shape. In analyzing MGS image E03-00824 we have found the Face to possess a very high degree of symmetry in two directions and

to contain subtle indications of an underlying geometrical plan based on rectangles having a long to short side ratio of 4/3. These new findings render previous criticisms concerning artificiality moot; i.e., that the Face cannot be a face and thus cannot be artificial because it doesn't look like a face. That our constructions seem to suggest a simple yet elegant geometry at a high level of confidence is difficult to explain as the result of some unknown naturally-occurring random process on Mars. The hypothesis that the Face on Mars is a highly symmetrical artificial object that appears as it does today due to the effects of erosion and deposition is simpler and more plausible than the hypothesis that it is a natural landform.

5. Summary and Recommendations

In April 2001, the Mars Global Surveyor was able for the first time to obtain a fully illuminated high resolution image of the Face on Mars landform in the Cydonia region. From this image a high resolution digital elevation model (DEM) was computed using shape-from-shading. Acquired about 25 degrees off nadir the DEM the MGS image was orthorectified using the DEM so as to appear as it would looking straight down. Analysis of the orthorectified image shows the Face to possess a very high degree of symmetry in two directions. Using repeatable constructions based on clearly resolved features the structure of the Face appears to fit a simple yet elegant geometrical model based on rectangles having a long to short side ratio of 4/3, i.e., by rectangles diagonally bisected by 3-4-5 right triangles. Analysis of the east side of the Face reveals that it is covered by dunes which have likely formed from sand blown by prevailing westerly winds and deposited on the leeward side. From 3-D perspective views this dune field appears to be covering much of the east side of the landform.

Because the east side appears covered with dunes, it is unlikely that optical imagery will provide much more useful data on the Face. Previously, L-band synthetic aperture radars have been flown aboard the Space Shuttle and used to map subsurface geological and archaeological features in the Eastern Sahara (McCauley et al 1982). Such radars can see features several meters below the surface. As an alternative to excavation, perhaps future Mars orbiters equipped with similar radars can be used to determine what is buried beneath the sand.

Appendix A Shape-from-Shading

Shape-from-shading is a method for generating 3-D digital elevation models (DEMs) from images. DEMs are used for orthorectifying images (Appendix B) and for generating 3-D views of the surface from different perspectives.

In computer graphics images are generated (rendered) from 3-D models. Shape-from-shading (SFS) is the inverse process of generating 3-D models from images. Both rely on a model of the image formation process. For Lambertian surfaces -- surfaces that reflect light equally in all directions -- the brightness in an image is related to the underlying surface by

$$i(x,y) = a\ R[p(x,y),q(x,y)]$$

where *R* is the reflectance map which models the reflectance properties of the surface, *p(x,y)* and *q(x,y)* are the gradients which describe the shape of the surface, and *a* is a constant that depends on the reflectivity of the surface, the sensitivity of the imaging system and other factors. This model assumes that the effects of atmospheric scattering have been removed.

A variety of methods have been developed for inverting the above equation -- for estimating the gradients from an image -- and for integrating the gradients (slopes) to form an elevation surface (Horn 1990). A simple method that provides satisfactory results in many planetary imaging scenarios based on some early ideas described by Horn (1977) is described below.

The reflectance map is a function that gives the brightness as a function of the gradients. For Lambertian surfaces the brightness is proportional to the cosine of the angle between the vector that is normal (perpendicular) to the surface and the vector in the direction of the light source. As noted by Pentland (1988), if the angle between the vector in the direction of the light source and the vector in the direction of the observer are more than 30 degrees apart and the surface is not too rough the reflectance map can be approximated by a linear relationship. If the image is rotated so that the vector that points to the sun is in the x-z plane, it can be shown that

$$i(x,y) = a[sin\ \phi\ p(x,y) + cos\ \phi]$$

where ϕ is the zenith angle of the sun. The constant of proportionality *a* is difficult to determine directly without ground truth (i.e., ground targets with known albedo and slope). However, since in most images the gradients are more-or-less uniformly distributed in all directions, the expected

value of the gradient in the x-direction *E[p]* can be assumed to be zero so the average image brightness

$$E[i] = a \cos \phi.$$

This then allows us to estimate the scale factor

$$a = E[i] / \cos \phi.$$

The elevation map *z(x,y)* can be obtained iteratively, row-by-row, summing along each row

$$z(x,y) = z(x\text{-}1,y) + [i(x,y) - a \cos \phi] / a \sin \phi$$

where *z(0,y)* are the boundary values. If the boundary values *z(0,y)* are unknown, we can minimize the mean-squared elevation difference between rows by subtracting the average elevation of a row from the elevations in that row.

Figure A-1a shows the height map (DEM) of a conical surface where brightness represents height, and a shaded rendition of the surface (Figure A-1b) viewed from below.
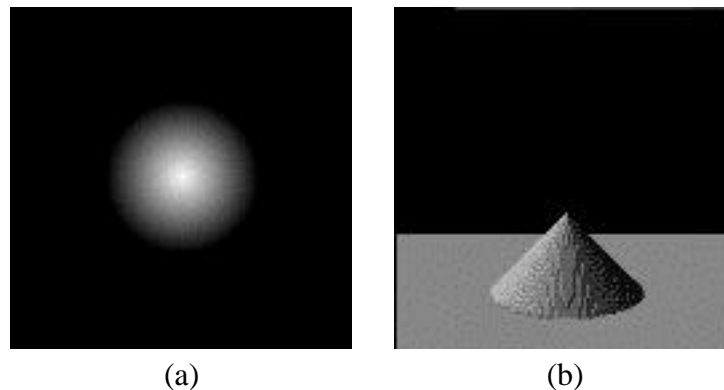

(a)   (b)

Figure A-1 DEM of a cone and a shaded perspective view

Figure A-2a is a synthetic image looking down on the cone with the light source directly overhead (ϕ = 0 deg.). Figure A-2b is the DEM estimated from the image using shape-from-shading. The poor performance of shape-from-shading at high illumination angles (low zenith angles) is like that experienced by image analysts who under similar conditions have difficulty in interpreting surface shape.
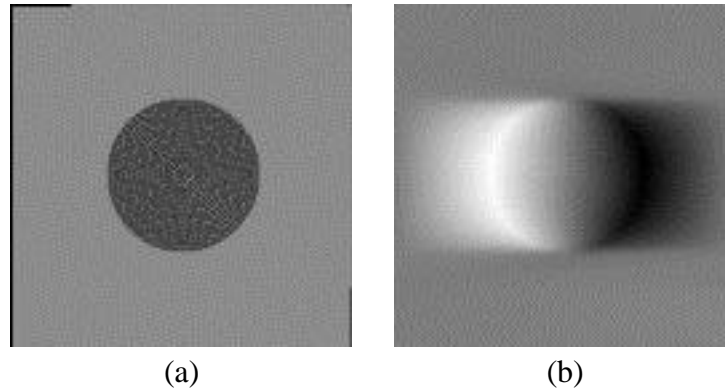
<center>(a)   (b)</center>

Figure A-2 Synthetic image of cone illuminated from directly above and the DEM estimated from it using shape-from-shading.

As the light source moves lower in the sky (zenith angle increases) performance improves. Figure A-3a shows a synthetic image generated with the light source to the left, 60 deg. above the horizon (ϕ = 30 deg.). Figure A3-b is the DEM estimated from that image.

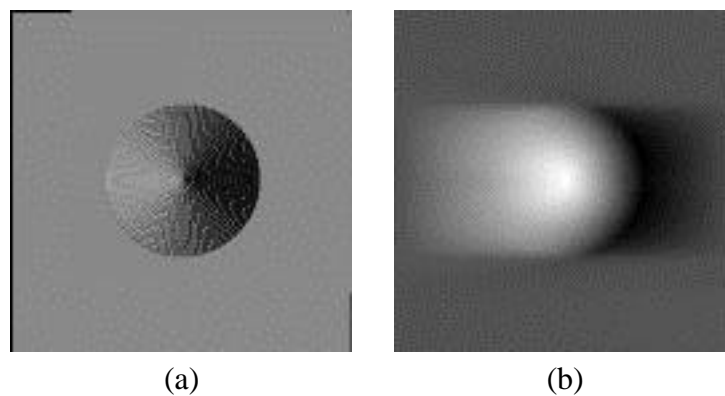

<center>(a)   (b)</center>

Figure A-3 Synthetic image of cone with light source at 60 deg. above the horizon and the DEM estimated from it using shape-from-shading.

As the zenith angle continues to increase the true shape of the surface begins to emerge. Figure A-4a is a synthetic image generated with the light source 30 deg. above the horizon. The estimated DEM (Figure A-4b) is very similar to the original surface (Figure A-1a).
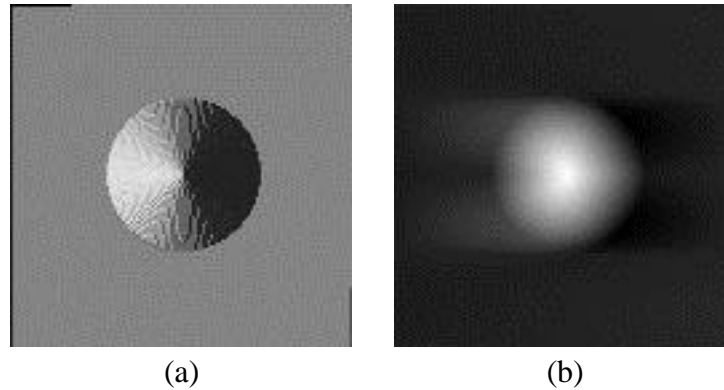
(a)   (b)

Figure A-4 Synthetic image of cone with light source at 30 deg. above the horizon and the DEM estimated from it using shape-from-shading.

Comparing perspective views of the original and estimated elevation surface from the last example (Figure A-5) shows the method capable of recovering the shape of the surface. The slight tilt in the surface in the direction of the light source (the sun) is a common artifact of this kind of algorithm.
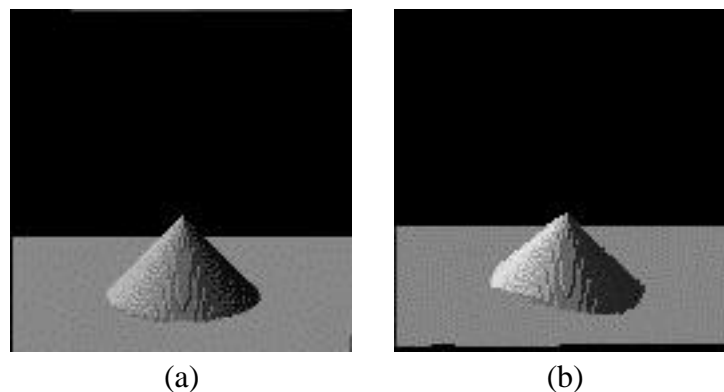

(a)   (b)

Figure A-5 Original shaded perspective view of cone (left) and estimated view computed by shape-from-shading (right)

The figure below compares Viking and MGS DEMs computed by shape-from-shading. Although the Viking and MGS images themselves are quite different due to differences in their lighting conditions and resolution, the derived DEMs are quite similar in structure. The diagonal striping pattern evident in the DEMs are an artifact of the shape from shading algorithm which generates the elevation surface by summing image brightness values in the direction of the sun.
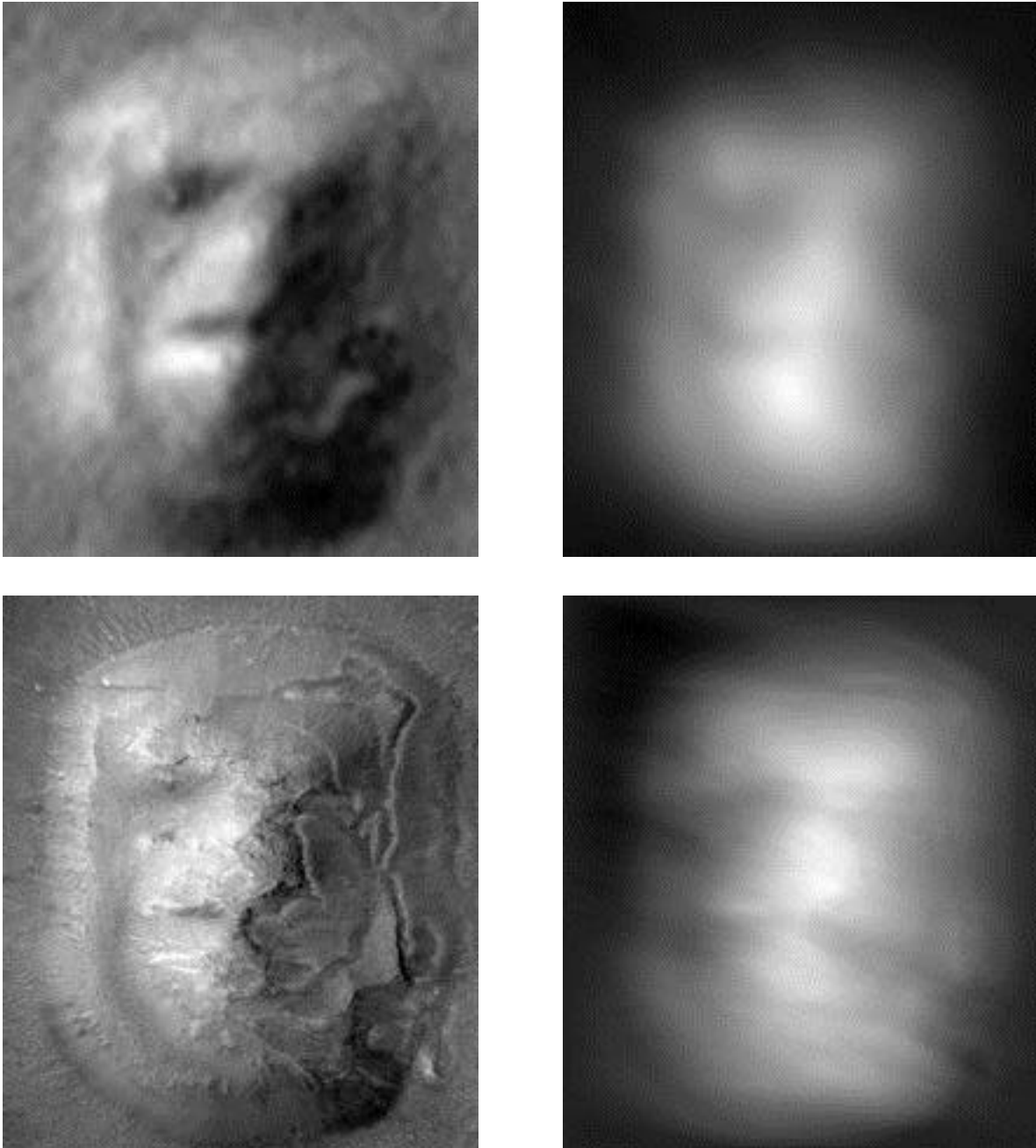
Figure A-6 Comparison of Viking and MGS derived DEMs and orthorectified images. Orthorectified Viking frame 70A13 (upper left) and DEM (upper right). Orthorectified MGS image E03-00824 (lower left) and DEM (lower right).

Appendix B - Orthorectification

When planetary surfaces are imaged obliquely (i.e., when the camera is looking off at an angle), the shape of objects on the ground are distorted. Correcting for these distortions is important in order to accurately analyze the symmetry and geometry of 3-D objects on the ground.
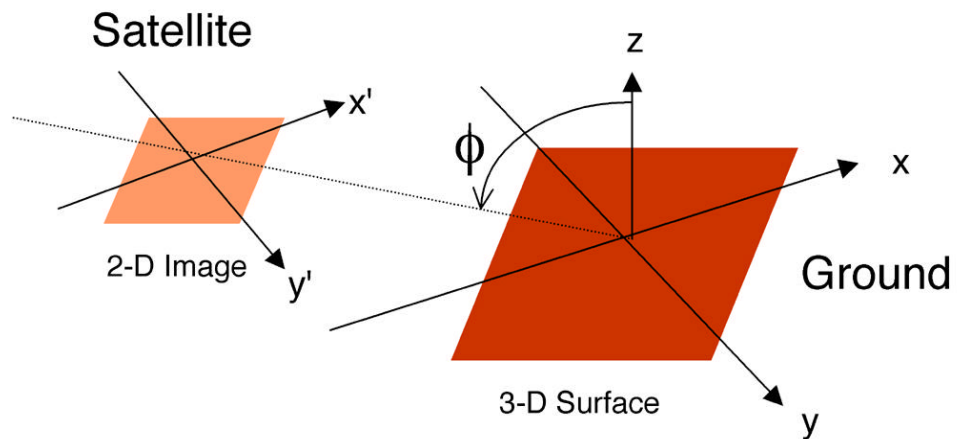

Figure B-1 Satellite imaging geometry

Image coordinates are related to their corresponding ground locations by means of a camera model. Usually the distance between a satellite and the surface is much greater than the variation in height of features on the surface over the region being imaged. If we define our coordinate system so that the *x* axis is in the direction of the satellite (Figure B-1), a point on the ground at location *(x,y)* and height *z* projects to the point *(x',y')* in the image according to (Foley and Van Dam 1983)

$$x' = x \cos \phi + z(x,y) \sin \phi$$
$$y' = y$$

where ϕ is the zenith angle of the satellite. If the camera on board the satellite is looking straight down ($\phi = 0$) the image is an orthographic projection of the scene ($x' = x,\ y' = y$). As the camera looks off to the side to image objects on either side of the orbital track, the zenith angle increases and the projection of the scene in the image plane is foreshortened (compressed) in the *x* direction by the factor *cos* ϕ. For example, if $\phi = 45$ degrees, the *x* dimension of the scene is compressed about 70% in the image. If the scene contains objects that are not flat, points at different heights must also be shifted by an amount that depends on their height.

Orthorectification is the process of reprojecting an oblique image to appear as if it were acquired from directly overhead. It reverses the oblique parallel projection, mapping the oblique view to the orthographic (overhead) view of the scene. Orthorectification can be accomplished by projecting the elevation map $z(x,y)$ to the oblique image plane

$$z(x',y') = z(xcos\ \phi + z(x,y)\ sin\ \phi,\ y)$$

and using it to backproject the oblique image

$$x = x'/cos\ \phi - z(x',y')\ tan\ \phi$$
$$y = y'.$$

The importance of orthorectification became evident initially in the process of analyzing the April 1998 MGS image of the Face (Carlotto et al 1999). Figure B-2 shows the original image (an oblique view) of the Face, a digital elevation model (DEM) derived from Viking image 35A72 projected to match the MGS view, and the orthorectified MGS image. JPL's geometrically stretched version of the Face which was widely disseminated over the Internet by JPL and the media is also shown for comparison. Because of the oblique viewing geometry of the MGS image, the left side of the Face appears wider than it really is while the right side appears narrower with much of it obscured by the central ridge. As shown in the figure orthorectification corrects for this effect while JPL's stretched version further distorts it (compare to Figure 3). Stretching an image to correct for foreshortening can be done only when the surface is flat. By not taking terrain into account, at a zenith angle of 45 degrees, internal features 400 meters above ground level are horizontally shifted 400 meters from their correct position. Because the Face is not flat, JPL's geometric stretch further distorts the internal structure of the Face, rendering it less face-like than it really is.
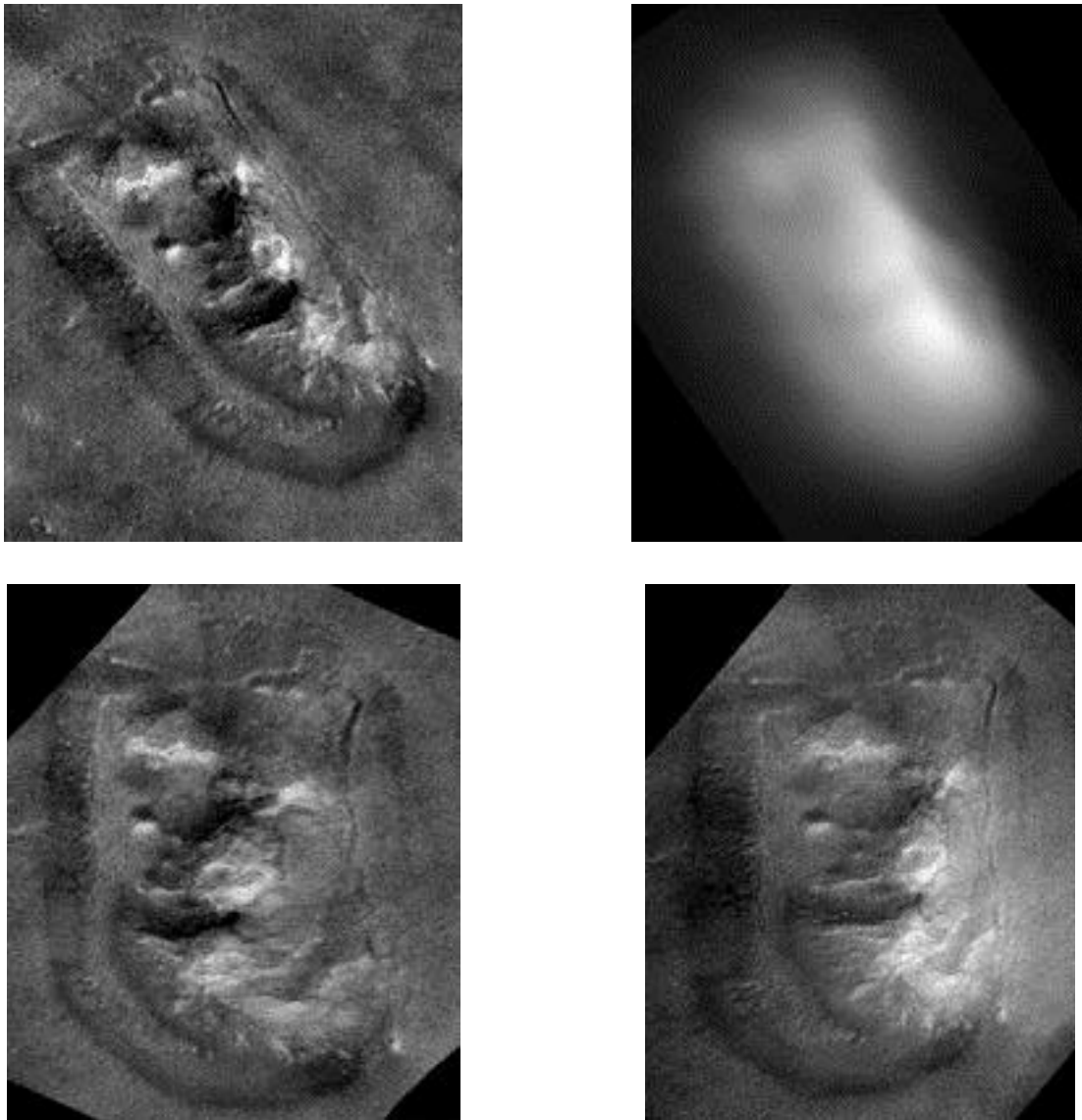
Figure B-2 Original MGS (upper left), Viking elevation model projected to MGS view (upper right), orthorectified image (lower left), and JPL's geometrically stretched image (lower right).

To more clearly illustrate the difference between simple geometrical stretching and orthorectification consider the following (Figure B-3) of the letter "A" on either a flat surface b) or non flat surface c). In an image of the object on a flat surface d) taken 45 degrees off angle from below, the object is foreshortened to 70% of its true height. In an image of the object on a non flat surface e) also taken 45 degrees off angle from below the internal structure of the object is distorted as well as foreshortened. If we try to correct e) assuming the surface is flat f) we obtain a poor approximation to its actual shape h). By using a model of the actual surface g) and orthorectifying the image a much better approximation i) to its true shape is obtained.
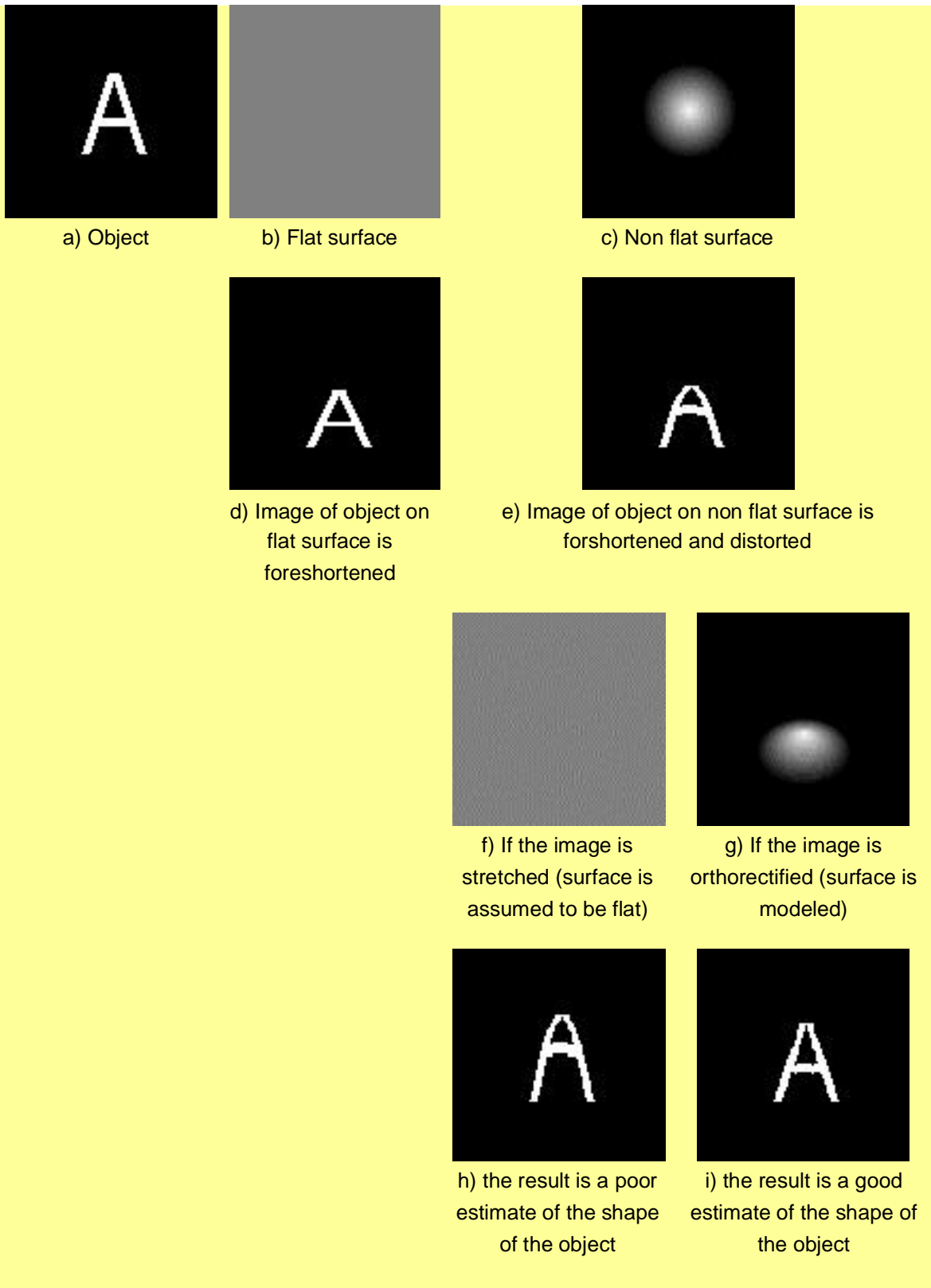
Figure B-3 Comparing the effects of simple geometrical stretching and orthorectification on images of 3-D objects.

Appendix C - Measuring Symmetry

Symmetry is defined with respect to a point or line. Mirror symmetry occurs when a line (axis of symmetry) passes through the object such that the two sides of the object are mirror images of each other. When the axis of symmetry is a vertical line, the object is said to be horizontally symmetrical; when the axis of symmetry is a horizontal line, the object is vertically symmetrical. With reference to Figure C-1, the letter "A" is horizontally symmetrical; "C" is vertically symmetrical. "Z" has no axis of symmetry, and "X" has two perpendicular axes of symmetry (horizontal and vertical). The letter "O" is symmetrical about all lines passing through its center point and is circularly symmetrical.
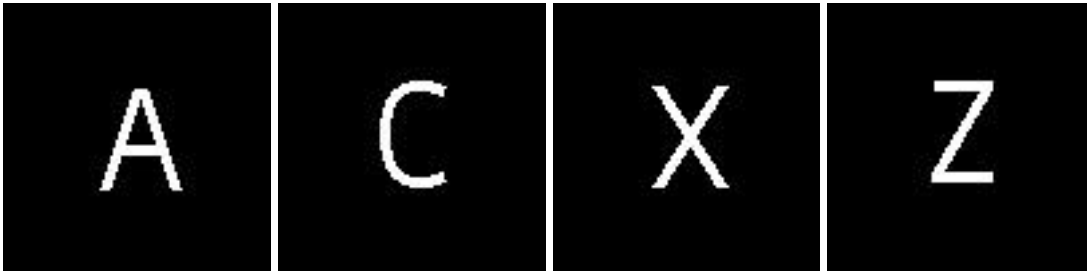

Figure C-1 Four letters used to illustrate horizontal and vertical symmetry

The Marola symmetry measure (Marola 1989) is the difference between the image of an object and its reflection about a hypothetical axis of symmetry. The difference is normalized to give values in the range from zero (no symmetry), to one (perfect symmetry). If $a(i,j)$ is an image, the Marola symmetry in the horizontal and vertical directions are:

$$\beta_h(m) = 1 - 1/2 \sum_{i,j} [a(i,j) - a(m-i,j)]^2 / \sum_{i,j} a^2(i,j)$$
$$\beta_v(n) = 1 - 1/2 \sum_{i,j} [a(i,j) - a(i,n-j)]^2 / \sum_{i,j} a^2(i,j)$$

where $0 \leq \beta \leq 1$. The axes of symmetry are given by the *(m, n)* value that maximizes the Marola symmetry.

Figure C-2 plots the Marola symmetry measure for the images of the letters "A", "C", "X", and "Z" in the horizontal (solid) and vertical (dotted) directions for different shifts. Peak values in a plot equal to one signify perfect symmetry in that direction. In general the letters are not exactly centered in the images and so the peaks do not always occur at a shift of zero. Clearly the Marola

symmetry measure is able to detect the horizontal symmetry of "A", the vertical symmetry of "C", the perpendicular (i.e., horizontal and vertical) symmetry of "X", and the lack of symmetry of "Z".
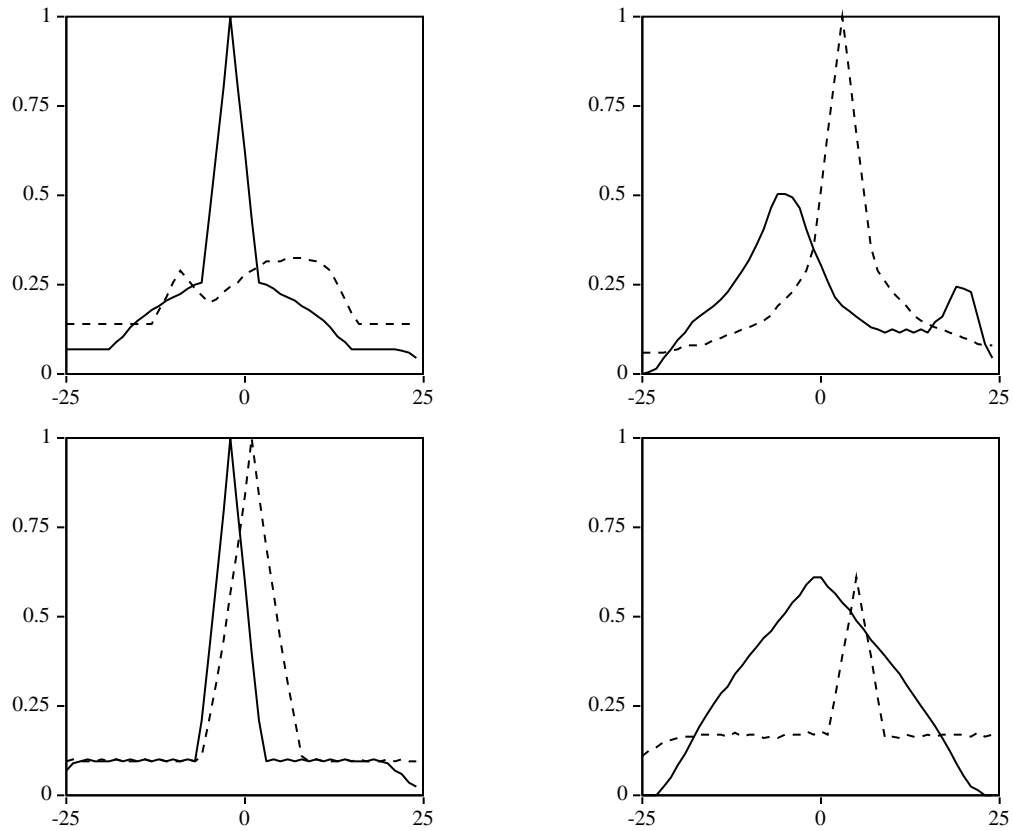

Figure C-2 Plots of the Marola symmetry measure for the letters "A" (upper left), "C" (upper right), "X" (lower left) and "Z" (lower right).

Appendix D Probability of Spatial Configurations

In order to assess the statistical significance of our geometric model of the Face the probability that a particular configuration of features can occur at random must be determined. We start by assuming the spatial distribution of features can be modeled as a Poisson process (Papoulis 1965).

a) Realization from a Poisson Process   *b) Linear configuration*

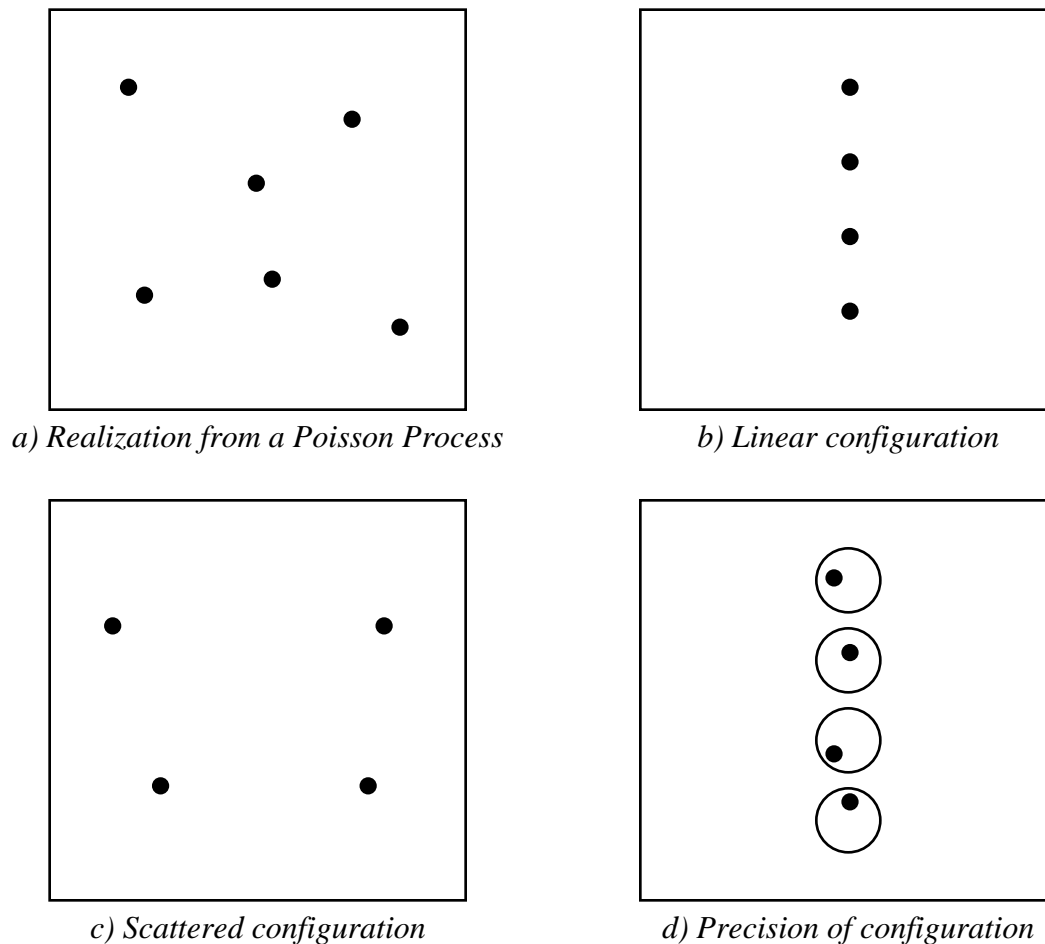*c) Scattered configuration*   *d) Precision of configuration*

Figure D-1 Modeling configurations of point features as a Poisson process

The probability that *k* point features occur within a given region of area *s* (Figure D-1a) is

$$p = (\lambda s)^k exp\text{-}\lambda s \ /k!$$

where λ is the feature density -- the number of features that occur on average per unit area. The probability of any specific configuration of k points is the same; e.g., the probability that four points will lie along a line (Figure D-1b) is the same as the probability that they are scattered (Figure D-1c).

Next we determine the probability that a configuration of points occurs at a given level of precision. The precision is controlled by allowing the points to be anywhere within circular regions of area t (Figure D-1d). The probability that a point is contained within one of these regions is $q=\lambda t exp-\lambda t$. If the regions do not overlap, the probability that all k points lie within their own predefined region of area t is q^k The likelihood ratio:

$$L = q^k/p = k!(t/s)^k \; exp \; -\lambda(kt-s)$$

gives the odds of a particular configuration of features occurring at random and depends on the precision of the configuration (defined by the area ratio t/s) and the number of features k. The likelihood decreases as the number of features increases, or as the size of the regions decreases regardless of the shape of the configuration.

We now consider the case of $k=3$ points within the Face at the intersections of 1) the horizontal and vertical axes of symmetry, 2) the upper half of ellipse **e1** with the horizontal axis of symmetry, and 3) the lower half of ellipse **e3** with the horizontal axis of symmetry. The likelihood that these points will all lie within the corresponding circular regions **a**, **b**, and **c** is q^3/p . If s is the total area of the Face (in plan view), and t the average area of the circular features, the ratios of the areas of circular features **a**-**c** to that of the Face itself are approximately 0.002, 0.002, and 0.001, respectively. Using t/s = 0.001, = 3, we obtain

$$L = 3!(0.001)^3 \; exp \; -3[3(.001)-1] \sim 1.2 \; x \; 10^{-7}.$$

This assumes that **a**-**c** are the only features of their kind within the Face. If we assume there are others, say 6 all together, then the density = 6 per unit area and we obtain

$$L = 3!(0.001)^3 \; exp \; -6[3(.001)-1] \sim 2.4 \; x \; 10^{-6}.$$

thus it would take on average one to ten million random trials before this configuration of points would occur.

References

M. J. Carlotto, "Digital imagery analysis of unusual Martian surface features," *Applied Optics*, Vol. 27, pp 1926-1933, 1988.

M. J. Carlotto and M.C. Stein, "A method for searching for artificial objects on planetary surfaces," *Journal of the British Interplanetary Society*, Vol. 43, pp 209-216, 1990.

Mark J. Carlotto, "Evidence in Support of the Hypothesis that Certain Objects on Mars are Artificial in Origin." *Journal of Scientific Exploration*, Vol. 11, No. 2 (Summer, 1997).

Mark J. Carlotto and John E. Brandenburg, "Analysis of Unusual Martian Surface Features: Enigmatic Geology or Archaeological Ruins?," *1999 Spring Meeting of the American Geophysical Union* (Poster Presentation), Boston, MA.

Mark. J. Carlotto, Horace W. Crater, James L. Erjavec, and Stanley V. McDaniel, "Response to Geomorphology of Selected Massifs On the Plains of Cydonia, Mars by David Pieri," *Journal of Scientific Exploration*, Vol. 13, No. 3, 1999.

M. Carr, *The Surface of Mars*, Yale University Press, New Haven CT, 1981.

V. DiPietro and G. Molenaar, *Unusual Martian Surface Features*, Mars Research, Glenn Dale MD, Fourth edition, 1988.

J. Erjavec and J. Brandenburg, "Evidence for a Paleo-Ocean Shoreline, Sedimentary Features and Water Erosion in Cydonia Mensae," *AGU Spring Meeting*, June 1-4, Boston MA, Abstract, P42A-10 (1999).

J. D. Foley and A. Van Dam, *Fundamentals of Interactive Computer Graphics*, Addison-Wesley, Reading, MA, 1983.

Richard C. Hoagland, *The Monuments of Mars: A City on the Edge of Forever*, Frog Limited/North Atlantic Books, Berkeley CA, 1996.

B. K. P. Horn, "Understanding image intensities," *Artificial Intelligence*, Vol. 8, pp 201-231, 1977.

B. K. P. Horn, "Hill shading and the reflectance map," *Image Understanding Workshop*, Palo Alto, CA 1979.

B. K. P. Horn, "Height and gradient from shading," *International Journal of Computer Vision*, Vol. 5, No. 1, 1990.

Jet Propulsion Laboratory, Caption of JPL Viking Press Release P-17384, July 31, 1976 (http://barsoom.msss.com/education/facepage/pio.html)

Willy Ley, *Rockets, Missiles, and Space Travel*, Viking Press, New York, 1951.

G. Marola, "On the detection of the axes of symmetry of symmetric and almost symmetric planar objects," *IEEE Trans. Pattern Analysis and Machine Intelligence*, Vol. 11, No. 1, Jan. 1989.

J.F. McCauley, G.G. Schaber, C.S. Breed, M.J. Grolier, C.V.Haynes, B.Issawi, C. Elachi, and R. Blom, Subsurface valleys and geoarcheology of the eastern Sahara revealed by Shuttle radar," *Science*, Vol. 218, pp 1004-1020, 1982.

S. V. McDaniel, *The McDaniel Report*, North Atlantic Books, Berkeley CA, 1994.

A. Papoulis, *Probability, Random Variables, and Stochastic Prcesses*, McGraw Hill, 1965.

A. Pentland, "The transform method for shape-from-shading," MIT Media Lab Vision Sciences Tech. Report 106, July 15, 1988.

D. C. Pieri, "Geomorphology of selected massifs on the plains of Cydonia, Mars," *Journal of Scientific Exploration*, Vol. 13, No. 3 (Fall, 1999).

Randolfo Pozos, "*The Face on Mars: Evidence for a Lost Civilization?*", Chicago Review Press, Chicago IL, 1986.

A. Sirisena, "Yes – There is a Face on Mars - But is it Artificial?" SPSR Technical Report, Society for Planetary SETI Research (http://24.31.153.81/spsr/articles/ReportForSPSR.htm)

H. Zabrodsky, S. Peleg, and D. Avnir, "Symmetry as a Continuous Feature," *IEEE Transactions on Pattern Analysis and Machine Intelligence*, Vol. 17, No. 12, Dec. 1995.

Mark J. Carlotto received B.S., M.S., and Ph. D. degrees in Electrical Engineering from Carnegie-Mellon University in 1977, 1979, and 1981. He has over 20 years of experience in satellite remote sensing and digital image processing. Dr. Carlotto has studied anomalous phenomena including unusual features on the moon, on Mars, and in space. His book, *The Martian Enigmas* describes in detail his analysis of imagery of the Face and other possible artificial objects on Mars imaged by a Viking Orbiter spacecraft in 1976. Dr. Carlotto has published over seventy papers in technical and scientific journals and conferences. His work has been reported in *New Scientist, Omni,* and *Newsweek,* and has appeared in numerous television programs including Carl Sagan's *Cosmos* series, *Sightings,* and *History's Mysteries.*